FEDERAL UNIVERSITY OF TECHNOLOGY, AKURE
JOURNAL OF ENGINEERING AND ENGINEERING TECHNOLOGY

ROBOTIC MANIPULATOR MODEL AND CONTROL ESTIMATION

Owojori, A. O.

Department of Electrical and Electronics Engineering, Federal University of Technology PMB 704, Akure, Ondo State, Nigeria

**Correspondence author: aoowojori@futa.edu.ng*

Owojori, A. O. (2025): Robotic Manipulator Model and Control Estimation. *FUTA Journal of Engineering and Engineering Technology /19(2), 80-87.*

Received Date: 15.08.25 **Accepted Date: 27.10.25**

Abstract
Mimicking the human arm functions in handling pick and place tasks within precise path or trajectory in a designed space has introduced the concept of arm manipulator robot control estimation. The system design involves an arm manipulator mounted on a fixed-base platform whose dynamics mathematical modelling is carried out on MATLAB/ Simulink software. Deploying the link kinematic model or Denavit-Hartenberg (DH) model followed by the Lagrangian equation to express the joint dynamics, a relatively precise mathematical model is obtained to address issues of geometrical configuration. MATLAB/ Simulink also allows the introduction of control actuators at different joints of the robot (three (3) servo motors in the arm manipulator). The control performance was estimated based on the joint angles of the arm manipulator system with respect to their torque inputs. A stable system response was obtained with settling time of 0.5 sec and Proportional-Integral-Derivative (PID) coefficients (φ_1: $K_p = 1.1772, K_i = 9.318,\ K_d = 0.03718$; φ_2: $K_p = 0.20862, K_i = 0.911, K_d = 0.0066$; φ_3: $K_p = 1.1772, K_i = 9.318, K_d = 0.0372$) for the arm joints.

Keywords: *Robotic system, MATLAB/Simulink, mathematical model, arm manipulator*

Introduction

Since the emergence of robots during industrial revolution up till date, technological advancement has continued to gain prominence capturing the mind of hobbyist, control experts and researchers (Kadis *et al*., 2010; Somefun *et al*., 2020; Owojori *et al*.,2024) with majority of their designs having human centric functions to carry out simple tasks. A sample of such system is the arm manipulator as shown in Figure 1, which operates based on the simple harmonic motion of a pendulum or inverted pendulum design. Critical study of the system involves kinematics with respect to a chosen coordinate (Koh and Cho, 1994; Snider, 2009; Yin and Pan, 2017), dynamics (Zhang *et al*., 2010), and ability for the system to attain practical stability.

Arm manipulator designs initially were made of mechanical control mechanisms, based on the principle of kinetic and potential energy conservation (Keuchel and Stephan, 19994; Owojori *et al*., 2024). The breakthrough in the industrial shift with various concepts adopted was further extended into areas of production and manufacturing of products which involves carrying out industrial processes such as used in bottling companies, and seaports amongst others. This simile complex machines incorporates the use of hydraulic, pneumatic, gearing and mechanical components (Luckel, 1995) for actuating and performing feedback control functions. Until recently, when electromechanical systems with large-scale electronics are used for actuating, driving and controlling industrial robots (Keuchel and Stephan, 1994). Arm manipulators provide platform for study of low-cost robots which can easily be scalable to varying tasks.

Practical stability is a major aspect of such system whose technologies has grown from basic theoretical concepts to advance concepts facilitating autonomous system design and can allow easy interfacing or interoperation with other robotic system. The n-link manipulator is structured to have revolute (R) or prismatic (P) joint configuration whose angular or linear displacement is proportional to the input control signal. Depending on the overall system configuration with respect to the near ground spatial motion, the system transfer function of the end effector with respect to the input signal is used to carryout control estimation of the system. Evaluating the time per every action taken and accurate tracking of such arm angle with respect to the command input is a major task in the design.

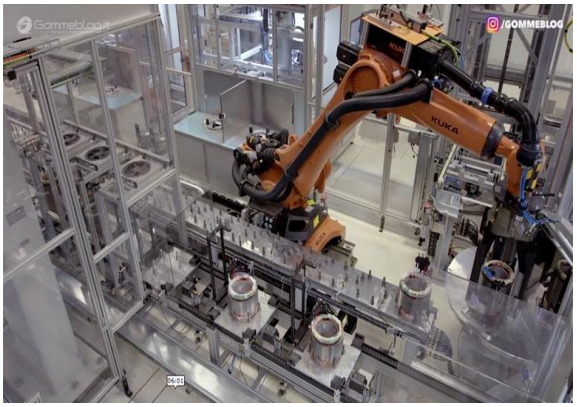

Figure 1: PKUKA Industrial Robot (Audi Electric Motor)

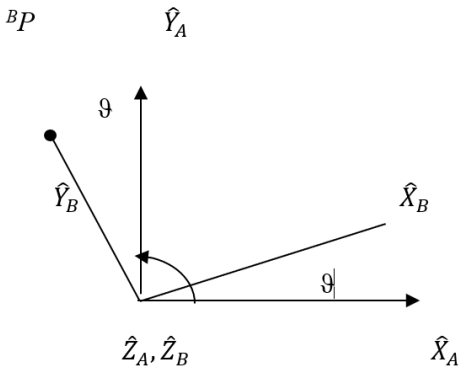

Figure 2: Rotation of frame {B} relative to frame {A} about $\hat{Z}$ axis

The major tasks have been approached over the years with the concept of time optimal control strategy and optimization algorithms which ensure minimal arrival time of the system end effector to the target area. In spite of all the approach used, the base line of proper analysis is still identified as the use a mathematical model or a CAD visualization model. This was carried out to keenly study the mechanical geometry (kinematic and dynamics) of the system after which effective electrical actuators and sensors were introduced interfaced with a programmable control unit. Similarly, an application software (SolidWorks CAD tool) installed on a personal computer (PC) was used to obtain a visual model of the robotic arm and with the MATLAB/Simulink application software control estimation on the models is carried out with intentions of obtaining a real-time system response via a Simulink/ Arduino Real-Time Operating System (RTOS) interface.

The fundamental derivation of the kinematic expressions for a physical model explores the 3-dimensional space, and expresses its corresponding relationship with other planes and coordinates in a well-ordered manner in terms of the position and orientation as shown in Figure 2 which illustrates the rotation of frame {B} relative to frame {A} about $\hat{Z}$ axis by an angular displacement ϑ.

In a universal coordinate system, the vector position of ^{A}P in three mutually orthogonal dimension (*X, Y, Z*) is expressed by Equation (1). The orientation of the body with reference to the coordinate system as described in coordinate system {B} relative to that of {A} shows a unit vector principal direction coordinates in {B} given as $\hat{X}_B, \hat{Y}_B$ and $\hat{Z}_B$, then the orientation with respect to the coordinate system {A}, are written as $^{A}X_B$, $^{A}Y_B$ and $^{A}Z_B$.

$$^{A}P = \begin{bmatrix} P_x \\ P_y \\ P_z \end{bmatrix} \tag{1}$$

On stacking the unit vectors together in a 3×3 column matrix, a rotational matrix ($^{A}_{B}R$) is formed which describes {B} relative to {A} as expressed in Equations (2-3). This helps in keeping track of mapping and frames of the reference.

$$^{A}_{B}R = [^{A}X_B \;\; ^{A}Y_B \;\; ^{A}Z_B] \tag{2}$$

$$^{A}_{B}R = \begin{bmatrix} \hat{X}_B.\hat{X}_A & \hat{Y}_B.\hat{X}_A & \hat{Z}_B.\hat{X}_A \\ \hat{X}_B.\hat{Y}_A & \hat{Y}_B.\hat{Y}_A & \hat{Z}_B.\hat{Y}_A \\ \hat{X}_B.\hat{Z}_A & \hat{Y}_B.\hat{Z}_A & \hat{Z}_B.\hat{Z}_A \end{bmatrix} = \begin{bmatrix} r_{11} & r_{12} & r_{13} \\ r_{21} & r_{22} & r_{23} \\ r_{31} & r_{32} & r_{33} \end{bmatrix} \tag{3}$$

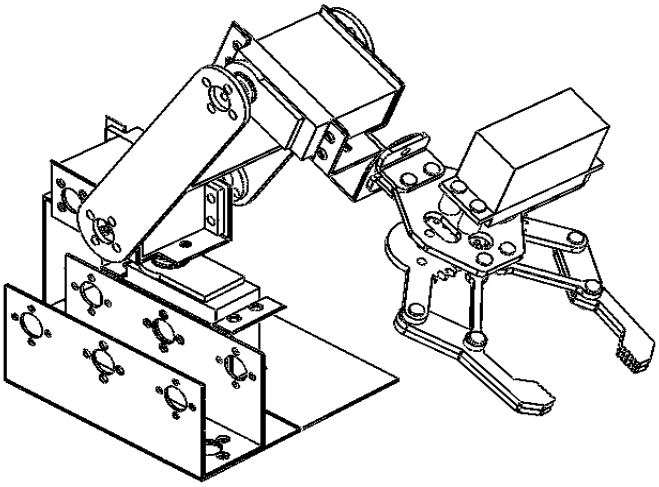

Figure 3: Arm Manipulator model

The dot product of unit vectors yields the cosine of the angle between the two axes; the rotation matrices are therefore often referred to as a direction cosine matrix which is further expressed in Equations (4-5)

$$\begin{cases} r_{ii} = \hat{X}_B.\hat{X}_A \\ \hat{X}_A = \hat{X}_B \cos\vartheta \\ r_{ii} = \hat{X}_B.\hat{X}_B \cos\vartheta \\ \hat{X}_B.\hat{X}_B = 1 \end{cases} \quad (4)$$

$$R_Z(\vartheta) = \begin{bmatrix} cos\,\vartheta & -sin\,\vartheta & 0 \\ sin\,\vartheta & cos\,\vartheta & 0 \\ 0 & 0 & 1 \end{bmatrix} \quad (5)$$

Hence, in dealing with a multilink system on different planes with angular displacement about different axis, the equivalent rotational matrix $({}^{A}_{B}R_{XYZ}(\gamma,\beta,\alpha))$ as it moves through X, Y, Z can be summarized as the product of the individual rotation in Equations (6-7). This expression can further be deployed in determining the position and orientation when given the joint angles (forward) and vis-versa (inverse) kinematics respectively of a multilink robot.

$${}^{A}_{B}R_{XYZ}(\gamma,\beta,\alpha) = R_Z(\alpha)R_Y(\beta)R_X(\gamma) \quad (6)$$

$$\begin{aligned} &{}^{A}_{B}R_{XYZ}(\gamma,\beta,\alpha) \\ &= \begin{bmatrix} cos\,\alpha & -sin\,\alpha & 0 \\ sin\,\alpha & cos\,\alpha & 0 \\ 0 & 0 & 1 \end{bmatrix} \begin{bmatrix} cos\,\beta & 0 & sin\,\beta \\ 0 & 1 & 0 \\ -sin\,\beta & 0 & cos\,\beta \end{bmatrix} \\ &\begin{bmatrix} 1 & 0 & 0 \\ 0 & cos\,\gamma & -sin\,\gamma \\ 0 & sin\,\gamma & cos\,\gamma \end{bmatrix} \end{aligned} \quad (7)$$

However, the article leveraged on the Denavit-Hartenberg (DH) model for the link kinematics followed by the Lagrangian equation to express the joint dynamics, which was expressed in MATLAB/ Simulink environment. The control performance was thereafter estimated based on the joint angles of the arm manipulator system with respect to their torque inputs.

Experimental Setup

This system identifies a four (4) degree of freedom robot reduced to three (3) degree of freedom revolute (3R) joint arm manipulator when the end effector joint was eliminated as shown in Figure 3. The general analytics of the system requires a study of the various part of the robot in space. As the multilink system increases such as on the same or different planes characterized with parallelogram linkages or other closed kinematic structures, a concept which makes use of the joint axes, and the link length in Denavit-Hartenberg (DH) structure could be adopted (Craig, 1989; Nwokah and Hurmuzlu, 2002; Lomai and Szederkenyi, 2008; Luo *et al*., 2020).

Hence, with the four parameters α_{i-1}, a_{i-1}, d_i, and ϑ_i, the reduced arm manipulator expressed in Table 1 was analysed to give a kinematic description of the robot as a transformation function of frame $\{i\}$ relative to frame $\{i-1\}$ as expressed in Equations (8-15).

$${}^{0}_{1}T = \begin{bmatrix} cos\,\varphi_1 & -sin\,\varphi_1 & 0 & 0 \\ sin\,\varphi_1 & cos\,\varphi_1 & 0 & 0 \\ 0 & 0 & 1 & 0 \\ 0 & 0 & 0 & 1 \end{bmatrix} \quad (8)$$

$${}^{1}_{2}T = \begin{bmatrix} cos\,\varphi_2 & -sin\,\varphi_2 & 0 & 0 \\ 0 & 0 & -1 & 0 \\ sin\,\varphi_2 & cos\,\varphi_2 & 0 & 0 \\ 0 & 0 & 0 & 1 \end{bmatrix} \quad (9)$$

$${}^{2}_{3}T = \begin{bmatrix} cos\,\varphi_3 & -sin\,\varphi_3 & 0 & l_a \\ sin\,\varphi_3 & cos\,\varphi_3 & 0 & 0 \\ 0 & 0 & 1 & 0 \\ 0 & 0 & 0 & 1 \end{bmatrix} \quad (10)$$

$${}^{0}_{3}T = {}^{0}_{1}T\,{}^{1}_{2}T\,{}^{2}_{3}T \quad (11)$$

Table 1: Reduced link kinematic description of the model

i	α_{i-1}	a_{i-1}	d_i	ϑ_i
1	0	0	0	φ_1
2	90	0	0	φ_2
3	0	l_a	0	φ_3

Table 2: Arm actuator specification of the model and Servo motor parameters

Servo/Metal frames, braces and link	Parameters
Manipulator robot	1.6 kg
Alloy handle weight	0.17 kg
Metal frame weight	0.057 kg
MG996RTowerPro DC Servo motor weight	0.057 kg
Torque	10 kg.cm
Current	1.7 A
Resistance (r_s)	3.9 Ω
Inductance (L)	12e^{-4} H
Back emf constant or Torque constant	6.876e^{-4} V/rpm
Inertia (J)	0.5 gcm^2
Torque damping coefficient (B_m)	1.5e^{-6} Nm/(rad/s)

Where $\cos\varphi_i$ *is* $c\varphi_i$ and $\sin\varphi_i$ *is* $s\varphi_i$

$$
{}^0_3T = \begin{bmatrix} c\varphi_1 c(\varphi_2+\varphi_3) & -c\varphi_1 s(\varphi_2+\varphi_3) & s\varphi_1 & l_a c\varphi_1 c\varphi_2 \\ s\varphi_1 c(\varphi_2+\varphi_3) & -s\varphi_1 s(\varphi_2+\varphi_3) & -c\varphi_1 & s\varphi_1 l_a c\varphi_2 \\ s(\varphi_2+\varphi_3) & c(\varphi_2+\varphi_3) & 0 & l_a s\varphi_2 \\ 0 & 0 & 0 & 1 \end{bmatrix} \quad (12)
$$

$$
{}^AP = {}^0_3T \begin{bmatrix} l_b \\ 0 \\ 0 \\ 1 \end{bmatrix} \quad (13)
$$

$$
\begin{bmatrix} c\varphi_1 c(\varphi_2+\varphi_3) & -c\varphi_1 s(\varphi_2+\varphi_3) & s\varphi_1 & l_a c\varphi_1 c\varphi_2 \\ s\varphi_1 c(\varphi_2+\varphi_3) & -s\varphi_1 s(\varphi_2+\varphi_3) & -c\varphi_1 & s\varphi_1 l_a c\varphi_2 \\ s(\varphi_2+\varphi_3) & c(\varphi_2+\varphi_3) & 0 & l_a s\varphi_2 \\ 0 & 0 & 0 & 1 \end{bmatrix} \begin{bmatrix} l_b \\ 0 \\ 0 \\ 1 \end{bmatrix} \quad (14)
$$

$$
\begin{bmatrix} x \\ y \\ z \\ 1 \end{bmatrix} = \begin{bmatrix} l_b c\varphi_1 c(\varphi_2+\varphi_3) + l_a c\varphi_1 c\varphi_2 \\ l_b s\varphi_1 c(\varphi_2+\varphi_3) + l_a s\varphi_1 c\varphi_2 \\ l_b s(\varphi_2+\varphi_3) + l_a s\varphi_2 \\ 1 \end{bmatrix} \quad (15)
$$

The mathematical model of this system is further expressed in Lagrange estimation to obtain the dynamic system analysis. The concept identifies the contribution of kinetic (E_K) and potential (E_P) energy in a system whereby expressing a Lagrange identifier (L) and its derivatives in Equations (16-17).

$$
L = E_K - E_P \quad (16)
$$

$$
\frac{d}{dt}\left(\frac{\partial L}{\partial \dot{\alpha}_i}\right) - \frac{\partial L}{\partial \alpha_i} = \tau_i \quad (17)
$$

$$
\ddot{\varphi}_1 = Num1/Den1
$$

$$
\begin{aligned} Num1 = 2(12a_1 &- 3gm_2\rho_2\cos(\varphi_1+\varphi_2+\varphi_3) \\ &- 3gm_1\rho_1\cos(\varphi_1+\varphi_2) \\ &- 6gm_2\rho_1\cos(\varphi_1+\varphi_2) \\ &- 3gm_2\rho_2\cos(\varphi_2-\varphi_1+\varphi_3) \\ &- 3gm_1\rho_1\cos(\varphi_1-\varphi_2) \\ &- 6gm_2\rho_1\cos(\varphi_1-\varphi_2) \\ &+ 3m_2{\rho_2}^2\dot{\varphi}_1\dot{\varphi}_2\sin(2\varphi_2 \\ &+ 2\varphi_3) \\ &+ 3m_2{\rho_2}^2\dot{\varphi}_1\dot{\varphi}_3\sin(2\varphi_2 \\ &+ 2\varphi_3) \\ &+ 3m_1{\rho_1}^2\dot{\varphi}_1\dot{\varphi}_2\sin(2\varphi_2) \\ &+ 12m_2{\rho_1}^2\dot{\varphi}_1\dot{\varphi}_2\sin(2\varphi_2) \\ &+ 12m_2\rho_1\rho_2\sin(2\varphi_2 \\ &+ \varphi_3)\dot{\varphi}_1\dot{\varphi}_2 \\ &+ 6m_2\rho_1\rho_2\sin(2\varphi_2 \\ &+ \varphi_3)\dot{\varphi}_1\dot{\varphi}_3 \\ &+ 6m_2\rho_1\rho_2\dot{\varphi}_1\dot{\varphi}_3\sin(\varphi_3)) \end{aligned}
$$

$$
\begin{aligned} Den1 = 2m_0{\rho_0}^2 &+ 3m_1{\rho_1}^2 + 12m_2{\rho_1}^2 \\ &+ 3m_2{\rho_2}^2 \\ &+ 3m_2{\rho_2}^2\cos(2\varphi_2 + 2\varphi_3) \\ &+ 3m_1{\rho_1}^2\cos(2\varphi_2) \\ &+ 12m_2{\rho_1}^2\cos(2\varphi_2) \\ &+ 12m_2\rho_1\rho_2\cos(\varphi_3) \\ &+ 12m_2\rho_1\rho_2\cos(2\varphi_2+\varphi_3) \end{aligned}
$$

$$
\ddot{\varphi}_2 = Num2/Den2
$$

$$Num2 = 24a_2 - 17m_2{\rho_2}^2\ddot{\varphi}_3 - 6gm_2\rho_2\cos(\varphi_1+\varphi_2+\varphi_3) - 6gm_1\rho_1\cos(\varphi_1+\varphi_2) - 12gm_2\rho_1\cos(\varphi_1+\varphi_2) - 9m_2{\rho_2}^2\cos(2\varphi_2+2\varphi_3)\ddot{\varphi}_3 + 6gm_2\rho_2\cos(\varphi_2-\varphi_1+\varphi_3) - 3m_2{\rho_2}^2{\dot{\varphi}_1}^2\sin(2\varphi_2+2\varphi_3) + 9m_2{\rho_2}^2{\dot{\varphi}_2}^2\sin(2\varphi_2+2\varphi_3) + 9m_2{\rho_2}^2{\dot{\varphi}_3}^2\sin(2\varphi_2+2\varphi_3) + 6gm_1\rho_1\cos(\varphi_1-\varphi_2) + 12gm_2\rho_1\cos(\varphi_1-\varphi_2) - 3m_1{\rho_1}^2{\dot{\varphi}_1}^2\sin(2\varphi_2) + 9m_1{\rho_1}^2{\dot{\varphi}_2}^2\sin(2\varphi_2) - 12m_2{\rho_1}^2{\dot{\varphi}_1}^2\sin(2\varphi_2) - 6m_2\rho_1\rho_2\cos(2\varphi_2+\varphi_3)\ddot{\varphi}_3 - 12m_2\rho_1\rho_2\sin(2\varphi_2+\varphi_3){\dot{\varphi}_1}^2 + 12m_2\rho_1\rho_2\sin(2\varphi_2+\varphi_3){\dot{\varphi}_2}^2 + 6m_2\rho_1\rho_2\sin(2\varphi_2+\varphi_3){\dot{\varphi}_3}^2 + 18m_2{\rho_2}^2\dot{\varphi}_2\dot{\varphi}_3\sin(2\varphi_2+2\varphi_3) - 18m_2\rho_1\rho_2\cos(\varphi_3)\ddot{\varphi}_3 + 18m_2\rho_1\rho_2{\dot{\varphi}_3}^2\sin(\varphi_3) + 12m_2\rho_1\rho_2\sin(2\varphi_2+\varphi_3)\dot{\varphi}_2\dot{\varphi}_3 + 36m_2\rho_1\rho_2\dot{\varphi}_2\dot{\varphi}_3\sin(\varphi_3)$$

$$Den2 = 17m_1{\rho_1}^2 + 24m_2{\rho_1}^2 + 17m_2{\rho_2}^2 + 9m_2{\rho_2}^2\cos(2\varphi_2+2\varphi_3) + 9m_1{\rho_1}^2\cos(2\varphi_2) + 36m_2\rho_1\rho_2\cos(\varphi_3) + 12m_2\rho_1\rho_2\cos(2\varphi_2+\varphi_3)$$

$$\ddot{\varphi}_3 = Num3/Den3$$

$$Num3 = 17m_2{\rho_2}^2\ddot{\varphi}_2 - 24a_3 + 6gm_2\rho_2\cos(\varphi_1+\varphi_2+\varphi_3) + 9m_2{\rho_2}^2\cos(2\varphi_2+2\varphi_3)\ddot{\varphi}_2 - 6gm_2\rho_2\cos(\varphi_2-\varphi_1+\varphi_3) + 3m_2{\rho_2}^2{\dot{\varphi}_1}^2\sin(2\varphi_2+2\varphi_3) - 9m_2{\rho_2}^2{\dot{\varphi}_2}^2\sin(2\varphi_2+2\varphi_3) - 9m_2{\rho_2}^2{\dot{\varphi}_3}^2\sin(2\varphi_2+2\varphi_3) + 6m_2\rho_1\rho_2\cos(2\varphi_2+\varphi_3)\ddot{\varphi}_2 + 6m_2\rho_1\rho_2\sin(2\varphi_2+\varphi_3){\dot{\varphi}_1}^2 - 6m_2\rho_1\rho_2\sin(2\varphi_2+\varphi_3){\dot{\varphi}_2}^2 - 18m_2{\rho_2}^2\dot{\varphi}_2\dot{\varphi}_3\sin(2\varphi_2+2\varphi_3) + 18m_2\rho_1\rho_2\cos(\varphi_3)\ddot{\varphi}_2 + 6m_2\rho_1\rho_2{\dot{\varphi}_1}^2\sin(\varphi_3) + 18m_2\rho_1\rho_2{\dot{\varphi}_2}^2\sin(\varphi_3)$$

$$Den3 = m_2{\rho_2}^2(9\cos(2\varphi_2+2\varphi_3)+17)$$

The system operation as a robotic manipulator when joints of the system are augmented with position actuators and sensors has parameters and specifications shown in Table 2.

Results and Discussion

The specifications and parameters depicted in Table 2 were used in MATLAB/Simulink model from which three angular positions $(\varphi_1(s), \varphi_2(s), \varphi_3(s))$ of the arm manipulator are obtained to track angles based on the set input reference. Using the PID controller with a step input perturbation in Figure 4, the response of the system converges at steady state output within settling time of 0.6 s accompanied with an initial overshoot of 0.98 (or 98%) for $\varphi_1(s)$, $\varphi_2(s)$ response also converges at steady state output within settling time of 0.6 s and 0.5 s, accompanied with an initial overshoot of 0.98 (or 98%) and 0.62 (or 62%) respectively. Similarly, $\varphi_3(s)$ response converges at steady state output within settling time of 0.6 s and 0.6 s, accompanied with an initial overshoot of 0.62 (or 62%) and 0.98 (or 98%) respectively. The response of the system viewed in a scope is shown in Figure 5 for the three angular positions of the arm manipulator system subjected to a unit step perturbation of 2 rads, 0.5 rads and 0.5 rads and specific trajectory using a signal builder within simulation time of 3 s.

From the PID gain concept, $Kcrit$ (1.962) and $Pcrit$ (0.2527) was chosen for $\varphi_1(s)$, $Kcrit$ (0.3477) and $Pcrit$ (0.458) for $\varphi_2(s)$, $Kcrit$ (0.2523) and $Pcrit$ (0.5054) for $\varphi_3(s)$ and these were used to design the controller gain parameters in Table 3 with the PID showing the best performance of convergence to the set reference when the value are multiplied by a constant ($\eta = 10000$). Although the result compared to the Auto-tuning PID in Figures (6-8) shows that at both parameters the closed loop system has stable response with the Ziegler-Nichols (Z-N). $\varphi_1(s)$ response shown in Figure 6 has a very quick rise time (0.00923 secs), settling time (0.106 secs) with a phase margin of 27.2^0 at 122 rad/s, gain margin of -25.6 dB at 16 rad/s and a higher maximum overshoot of 54.3% as compared to the auto-tuning PID.

$\varphi_2(s)$ response however shown in Figure 7 shows relative close rise time (0.0516 s), settling time (0.873 s) with a phase margin of 27^0 at 20.9 rad/s, gain margin of -9.57 dB at 11.5 rad/s and a higher maximum overshoot of 54.3% as compared to the auto-tuning PID.

While $\varphi_3(s)$ response shown in Figure 8 shows quick rise time (0.00583 s), settling time (0.404 s) with a phase margin of 23.6^0 at 216 rad/s, gain margin of -25.4 dB at 8.27 rad/s and a higher maximum overshoot of 38.4% as compared to the auto-tuning PID.

The overall gain controller for the arm manipulator is summarized in Table 3 establishing a stable system response with Proportional-Integral-Derivative (PID) coefficients (φ_1: $K_p =$

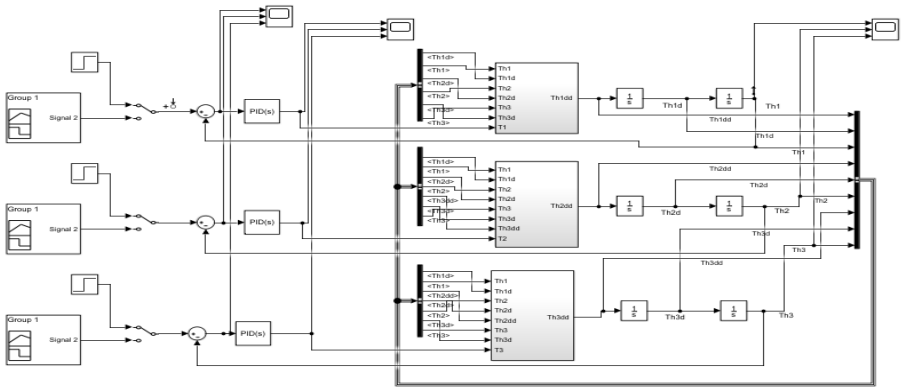

Figure 4: Arm manipulator model with PID controller

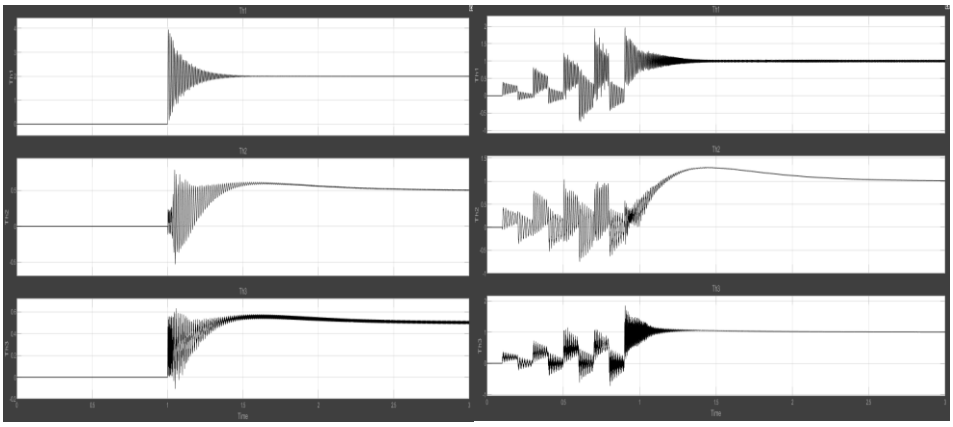

Figure 5: Basic control system block with unity feedback

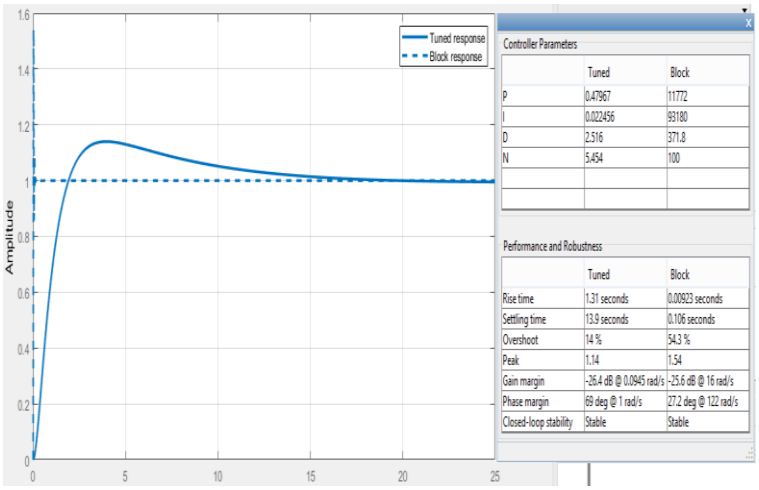

Figure 6: Comparison between the Z-N and Auto-tuning PID for $\varphi_1(s)$

$1.1772, K_i = 9.318, \quad K_d = 0.03718; \quad \varphi_2: K_p = 0.20862, K_i = 0.911, K_d = 0.0066; \; \varphi_3: K_p = 1.1772, K_i = 9.318, K_d = 0.0372)$ for the arm joints.

Conclusions

This article gives a conceptual arm manipulator robot control estimation on a fixed-base platform. The link kinematic model adopted the Denavit-Hartenberg (DH) model followed by the Lagrangian equation to express the joint dynamics was used, thereby obtaining a relatively precise mathematical model that addresses issues of geometrical configuration. MATLAB/ Simulink modelled derived from the expressions assumed the actuators at different joints of the robot (three (3) servo motors in the arm manipulator) are consistent hence a unity forward path was used. The control performance was estimated based on the joint angles of the arm manipulator system with respect to their torque

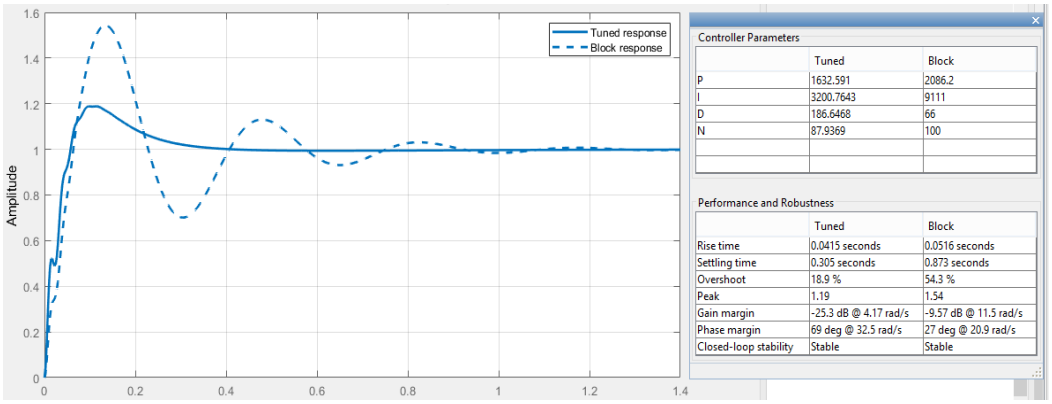

Figure 7: Comparison between the Z-N and Auto-tuning PID for $\varphi_2(s)$

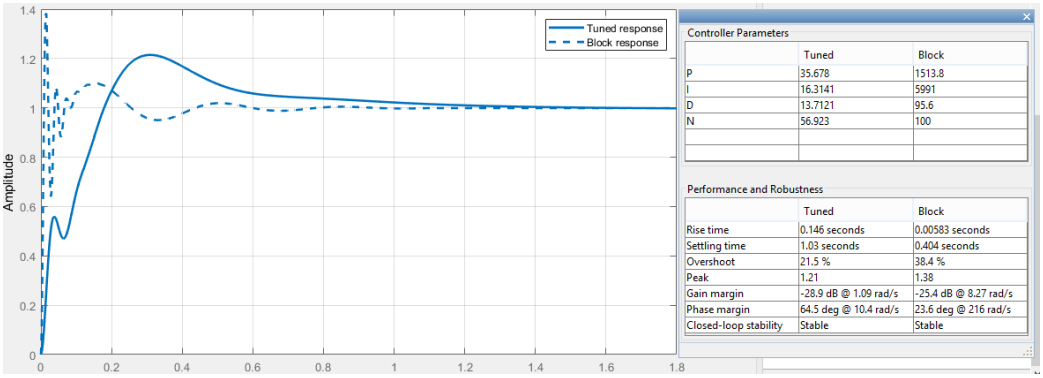

Figure 8: Comparison between the Z-N and Auto-tuning PID for $\varphi_3(s)$

Table 3: Arm manipulator Controller Gain Parameters

		K_p	T_i	T_d
	P	0.981		
Th1	**PI**	0.8829	$0.21056(K_i = 4.193)$	
	PID	1.1772	$0.12634(K_i = 9.318)$	$0.03158(K_d = 0.03718)$
	P	0.17385		
Th2	**PI**	0.156465	$0.381(K_i = 0.411)$	
	PID	0.20862	$0.22898(K_i = 0.911)$	$0.03158(K_d = 0.0066)$
	P	0.12615		
Th3	**PI**	0.113535	$0.4211(K_i = 0.2696)$	
	PID	0.15138	$0.2527(K_i = 0.5991)$	$0.06317(K_d = 0.00956)$

inputs. For the derivation of three angular positions of the arm manipulator 2 rads, 0.5 rads and 0.5 rads were used to specify trajectory using a signal builder within simulation time of 3 s. A stable system response was obtained with settling time of 0.5 sec and Proportional-Integral-Derivative (PID) coefficients (φ_1: $K_p = 1.1772, K_i = 9.318,\ K_d = 0.03718$; φ_2: $K_p = 0.20862, K_i = 0.911, K_d = 0.0066$; φ_3: $K_p = 1.1772, K_i = 9.318, K_d = 0.0372$) which shows better response than the P and PI controller configuration.

References

Craig, J. J. (1989) Introduction to Robotics, Mechanics and Control. 2nd Edition.

Kadis, A., Caldecott, D., Edwards, A., Jerbic, M., Madigan, R., Haynes, M., Cazzolato, B. and Prime, Z. (2010) Modelling, Simulation and Control of an Electric Unicycle. University of Adelaide.

Keuchel, U. and Stephan, R. M. (1994) Microcontroller-Based Adaptive Control

Applied to Thyristor-Driven DC-Motors. Springer-Verlag London.

Koh, K. C. and Cho, H. S. (1994) A path tracking control system for autonomous mobile robots: an experimental investigation. *Elsevier Science Ltd*, Great Britain 4(8), 799-820.

Lomai, F. and Szederkenyi, G. (2008) Trajectory Tracking Control of a 6-Degree of Freedom Robot Arm using Nonlinear Optimization. *IEEE Journal*. 655-660.

Luckel, J. (1995) From Design Methods to Industrial Applications. Proceedings of the Third Conference on Mechatronics and Robotics. *Springer Fachmedien Wiesbaden*.

Luo, C., He, Y. and Abubakar, S. (2020) Solving Inverse Kinematics of the Shotcrete Manipulator Based on the Plane Two-link Model and Trajectory Planning. Journal of Robotics, Hindawi, 1-12.

Nwokah, O. D. I. and Hurmuzlu, Y. (2002) The Mechanical Systems Design Handbook: Modeling, Measurement and Control. The Electrical Engineering Handbook Series. *CRC Press LLC*. 1-819.

Owojori, A.O., Akingbade, K.F., Apena, W.O. and Ogunti, E.O. (2024) Dynamic Model Comparison and Stability Control Design of a Differential Drive Robot. *Journal of Engineering and Engineering Technology.* 18(1), 41-49.

Snider, J. M. (2009) Automatic Steering Methods for Autonomous Automobile Path Tracking.

Somefun, O. A., Akingbade, K. F. and Dahunsi, F. M. (2020) Speed Control of DC Motors: Optimal Closed PID-Loop Model Predictive Control. *Universal Journal of Control and Automation*. 8(1), 9-21.

Yin, X. and Pan, L. (2017). Direct adaptive robust tracking control for 6 DOF industrial robot with enhanced accuracy. *ISA Transaction, Elsevier*. 1-7.

Zhang, W., Zhao, D., Chen, Q. and Du, D. (2010) Linkage underactuated humanoid robotic and with control of grasping force. *2nd International Asia Conference on Informatics in Control, Automation and Robotics*.